Viscosity and phase state of wildfire smoke particles in the stratosphere from pyrocumulonimbus events: an initial assessment

Authors:

Mei Fei Zeng,[1] Andreas Zuend,[2] Nealan G.A. Gerrebos,[1] Pengfei Yu,[3] Gregory P. Schill,[4] Daniel M. Murphy,[4] Allan K. Bertram[1]*

1. Department of Chemistry, The University of British Columbia, Vancouver, BC, V6T 1Z1, Canada

2. Department of Atmospheric and Oceanic Sciences, McGill University, Montreal, QC, H3A 0B9, Canada

3. Institute of Environmental and Climate Research, Jinan University, Guangzhou, 511443, China.

4. National Oceanic and Atmospheric Administration, Chemical Sciences Laboratory, Boulder, CO, 80305, USA.

*bertram@chem.ubc.ca

https://doi.org/10.26434/chemrxiv-2024-27934-v4 **ORCID:** https://orcid.org/0000-0002-5621-2323 Content not peer-reviewed by ChemRxiv. **License:** CC BY 4.0

Abstract.

Understanding the viscosity and phase state of biomass-burning organic aerosol (BBOA) from wildfires and pyrocumulonimbus (pyroCb) events in the stratosphere is critical for predicting their role in stratospheric multiphase chemistry and ozone depletion. However, the viscosity and phase state of BBOA under stratospheric conditions, including interactions with sulfuric acid (H_2SO_4), remain largely unquantified. In this study, we combine laboratory data with a thermodynamic model to predict the viscosity and phase state of BBOA under stratospheric conditions. Our results suggest that BBOA with a H_2SO_4-to-BBOA mass ratio of 0.37—an estimated upper limit for pyroCb smoke in the lower stratosphere after two months of aging— is highly viscous and frequently exists in a glassy state. Even at a higher H_2SO_4-to-BBOA mass ratio of 0.79 – an estimated upper limit after nine months of aging – BBOA can still transition to a glassy state under certain stratospheric conditions. In the glassy state, bulk reactions are suppressed, and multiphase chemistry may be limited to the particle surfaces. We also highlight key areas for future research needed to better constrain the viscosity and phase state of BBOA in the stratosphere and its subsequent impact on ozone.

Keywords: Aerosols, biomass burning, viscosity, phase state, glass state, polar stratospheric clouds, ozone layer, oxidation, atmospheric aging

Synopsis statement: Biomass-burning organic aerosol from wildfires can exist in a glassy state in the stratosphere, which can affect multiphase chemistry, polar stratospheric cloud formation, and ozone depletion predictions.

1. Introduction:

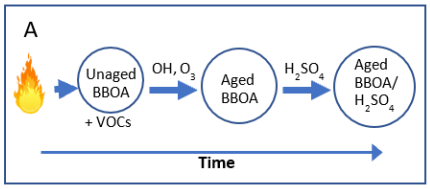

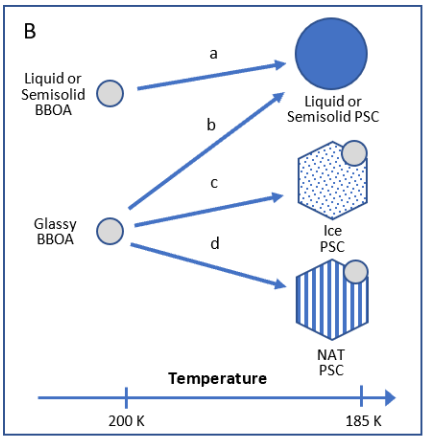

https://doi.org/10.26434/chemrxiv-2024-27934-v4 **ORCID:** https://orcid.org/0000-0002-5621-2323 Content not peer-reviewed by ChemRxiv. **License:** CC BY 4.0

Figure 1. *A) Aging of biomass burning organic aerosol (BBOA) in the stratosphere. VOCs represent volatile organic compounds. B) Possible formation pathways of polar stratospheric clouds (PSCs). NAT represents nitric acid trihydrate. PSCs form at temperatures less than ≅ 200 K.*

Large wildfires periodically inject massive amounts of smoke into the stratosphere (~15 km ≤ altitude ≤ 50 km) via pyrocumulonimbus (pyroCb) events and associated deep convection. Examples include the large-scale wildfires in the Pacific Northwest of North America in 2017 and the Australian "black summer" fires in 2019 — 2020.[1,2] Smoke is also ubiquitous in the upper troposphere and is mixed into the lowermost stratosphere.[3,4]

Smoke from wildfires consists of mostly organic aerosol, called biomass-burning organic aerosol (BBOA).[5] For example, smoke sampled from wildfires in the western U.S.A. comprised of > 90% BBOA by mass.[6,7] Wildfires also emit large amounts of volatile organic compounds (VOCs). In the atmosphere, hydroxyl radicals (OH) and ozone (O_3) oxidize VOCs, and some of the products of these reactions condense onto existing particles, adding to the BBOA mass.[8] OH and O_3 can also react directly with BBOA, forming a more oxidized aerosol. These combined processes result in aged BBOA (Fig. 1A).

In the stratosphere, sulfuric acid (H_2SO_4) can also condense on to the aged BBOA to form aged BBOA-H_2SO_4 particles (Fig. 1A). The sources of H_2SO_4 in the stratosphere includes the oxidation of sulfur dioxide (SO_2) from pyroCb events and volcanic eruptions and the oxidation of carbonyl sulfide (COS) from natural and industrial sources.[3,9–11] The conversion of SO_2 to H_2SO_4 occurs on the order of several weeks in the stratosphere,[12] while the conversion of COS to H_2SO_4 occurs on the order of tens of years.[11]

BBOA can linger for many months in the stratosphere and contribute to the depletion of the UV-blocking stratospheric ozone layer.[13–15] Key reactions that may occur on BBOA in the stratosphere and contribute to stratospheric ozone depletion include $ClONO_2$+HCl, $ClONO_2$+H_2O, and HOCl+HCl.[16] These reactions on BBOA could delay ozone layer recovery for years to come, increasing ultraviolet radiation exposure at the Earth's surface and raising the risk of skin cancer.[14,15] Additionally, BBOA introduced into the stratosphere by pyroCb events may influence the formation of polar stratospheric clouds (PSCs), potentially causing further depletion of the stratospheric ozone layer.[17]

Two Important properties of BBOA are the viscosity and phase state (i.e., liquid, semisolid, or amorphous solid). These properties are closely related: liquids have a viscosity < 10^2 Pa s, semisolids range from 10^2 — 10^{12} Pa s, and amorphous ("glassy") solids exhibit a viscosity > 10^{12} Pa s.[18]

Knowledge of the viscosity and phase state of BBOA particles is needed to predict the rates of multiphase reactions, including the multiphase reactions mentioned above that can contribute to ozone depletion.[19–22] For example, the rate for a multiphase reaction often depends on the square root of the diffusion coefficient within the aerosol particle.[16] Since diffusion is related to 1/viscosity, this implies that the rate often depends on the square root of 1/viscosity.

https://doi.org/10.26434/chemrxiv-2024-27934-v4 **ORCID:** https://orcid.org/0000-0002-5621-2323 Content not peer-reviewed by ChemRxiv. **License:** CC BY 4.0

Consequently, high viscosities and the glassy state could inhibit multiphase reactions within the particle bulk, restricting multiphase chemistry to the particle surface.

Knowledge of the viscosity and phase state of BBOA is also needed to predict the formation pathways of PSCs (Fig. 1B). If BBOA particles are in a non-glassy state, they can take up H_2O and HNO_3 at low temperatures to form non-glassy PSCs (pathway a). In addition, Ansmann et al. speculated that BBOA particles in a glassy state could heterogeneously nucleate crystalline ice or crystalline nitric acid hydrate (NAT) (pathways c and d).[17] We also speculate that glassy BBOA may take up H_2O and HNO_3 to form non-glassy PSCs due to the plasticizing effect of small molecules like H_2O and HNO_3 (pathway b).

Researchers previously measured or estimated the viscosity and phase state of BBOA as a function of temperature and relative humidity (RH).[19,20,23,24] They used these results to predict the behavior of BBOA in the troposphere (altitude $\lesssim$ 15 km). However, the temperature and RH in the stratosphere differ substantially from those in the troposphere, and these differences can strongly impact viscosity and phase state (as discussed below). Additionally, no studies have quantified the effect of H_2SO_4 uptake, or the uptake of any inorganic species, on BBOA viscosity and phase state. In a recent modelling study of stratospheric chemistry, researchers assumed that BBOA-H_2SO_4 particles in the stratosphere exist in a non-glassy state, allowing reactions to occur in the bulk of the particles.[14,15] However, this assumption has not been verified with experiments or calculations. As a result, the viscosity and phase state of BBOA under stratospheric conditions remain highly uncertain.

Several previous studies have quantified the viscosity and phase state of secondary organic aerosol (SOA) in the troposphere. These studies show that SOA, when free of inorganic species, can exist in a glassy state in the upper troposphere.[25–27] However, these studies did not consider the temperatures and RH in the stratosphere, and most did not consider the uptake of inorganic species, such as H_2SO_4.[28]

In the following, we use laboratory data and a thermodynamic model to predict the viscosity and phase state of BBOA in the stratosphere from pyroCb events. We focus on altitudes from 15 — 32 km in the stratosphere, since wildfire plumes from pyroCb events have been observed at these altitudes. [29–31] We first estimate the viscosity and phase state for unaged BBOA at these heights. Next, we estimate the viscosity and phase state of aged BBOA particles mixed with H_2SO_4 (aged BBOA-H_2SO_4 particles) at these heights. The implications of the results for stratospheric chemistry and PSCs are discussed, as well as observational constraints of the viscosity and phase state of BBOA in the stratosphere. We also provide an outlook for future research on the viscosity and phase state of BBOA in the stratosphere.

2. Methods.

2.1 Temperature in the stratosphere relevant for BBOA from pyroCb events.

The viscosity of organic aerosols depends strongly on temperature. Simulated zonal mean monthly temperatures for January and July were obtained from the Whole Atmosphere Community Climate Model (WACCM) for the year 2000 (see Fig. S1).[32,33] WACCM has

https://doi.org/10.26434/chemrxiv-2024-27934-v4 ORCID: https://orcid.org/0000-0002-5621-2323 Content not peer-reviewed by ChemRxiv. License: CC BY 4.0

72 vertical levels from surface to about 140 km above surface level and a horizontal resolution of 1.9° latitude by 2.5° longitude.

[29–31] For the altitude range of 15 — 32 km, the stratospheric temperatures vary from 177 — 250 K (see Fig. S1). As a result, we will focus on this temperature range throughout the remainder of this article.

2.2 RH in the stratosphere relevant for BBOA from pyroCb events.

The viscosity of organic aerosols depends strongly on the RH. The RH in the stratosphere was calculated using the following equation:

$$RH = \frac{P_w}{P_w^*} \times 100\%, \quad (1)$$

where P_w is the atmospheric water vapour pressure and P^*_w is the equilibrium (saturation) water vapour pressure over liquid water. P_w was calculated using the following equation:

$$P_w(z) = C_{H2O} \times P_{total}(z), \quad (2)$$

where z represents altitude and C_{H2O} represents the mixing ratio of water vapor in air. $P_{total}(z)$ represents the total atmospheric pressure at z and was calculated using a scale height (H) of 7.4 km and the barometric law:

$$P_{total}(z) = 101325\ Pa \times \exp\left(-\frac{z}{H}\right), \quad (3)$$

P^*_w was calculated using the following equation from Murphy and Koop:[34]

$$P^*_{H_2O}(T) = \exp\left(54.84276 - \frac{6763.22}{T} + \tanh\{0.01415(T - 218.8)\}\left[53.878 - \frac{1331.22}{T} - 9.4452\ln(T) \times \exp(-4.210\ln(T) + 0.014392T)\right]\right), \quad (4)$$

where T represents temperature.

Typical C_{H2O} values in the stratosphere are approximately 5 ppmv. However, elevated levels have been observed in wildfire plumes transported to the stratosphere through pryoCb events. Kablick et al. reported C_{H2O} values exceeding 15 ppmv in plumes from the Australian wildfires during 2019 —2020,[29] and Yu et al. observed C_{H2O} values exceeding 5 ppmv in plumes from Canadian wildfires in 2017.[35] To align with these observations, we focus on C_{H2O} values of 15 ppmv in our analysis.

2.3 Viscosity of unaged BBOA

https://doi.org/10.26434/chemrxiv-2024-27934-v4 ORCID: https://orcid.org/0000-0002-5621-2323 Content not peer-reviewed by ChemRxiv. License: CC BY 4.0

Table 1. *BBOA types and their properties used to determine the viscosity of unaged BBOA in the stratosphere. Relevant properties are the glass transition temperatures of dry BBOA ($T_{g,BBOA}$) and the volume-based hygroscopicity factor (κ).*

BBOA type	Reference	$T_{g,BBOA}$	κ
Pine wood BBOA generated from flaming	Xu et al.[23]	275.3 K[a]	0.129[e]
Poplar wood BBOA generated from flaming	Xu et al.[23]	269.1 K[a]	0.079[e]
Cedar wood BBOA generated from flaming	Xu et al.[23]	273.3 K[a]	0.116[e]
Water soluble component of pine wood BBOA generated from smoldering	Schnitzler et al.[19]	258.8 K[b]	0.071[f]
Hydrophobic phase of pine wood BBOA generated from smoldering	Gregson et al.[20]	230.0 K[b]	0.0003[f]
Hydrophilic phase of pine wood BBOA generated from smoldering	Gregson et al.[20]	240.0 K[b]	0.031[f]
Subalpine fir BBOA generated from flaming	DeRieux et al.[24]	286.0 K[c]	0.1[g]
Subalpine fir BBOA generated from flaming	DeRieux et al.[24]	254.0 K[d]	0.1[g]
Lodgepole pine BBOA generated from flaming	DeRieux et al.[24]	277.0 K[c]	0.1[g]
Lodgepole pine BBOA generated from flaming	DeRieux et al.[24]	266.0 K[d]	0.1[g]

[a]Glass transition temperature determined from volatility measurements.
[b]Glass transition temperature determined from viscosity measurements.
[c]Glass transition temperature determined from mass spectra recorded with electrospray ionization mass spectrometry.
[d]Glass transition temperature was determined from mass spectra recorded with atmospheric pressure photoionization mass spectrometry.
[e]Value calculated from oxygen-to-carbon (O/C) atomic ratios of the BBOA and following the parameterization provided by Lambe et al.[36]
[f]Value determined from RH-dependent viscosity data of the BBOA.
[g]Value used previously for this BBOA.

The glass transition temperature of dry BBOA ($T_{g,BBOA}$) and the volume-based hygroscopicity parameter of the BBOA (κ) have been reported for several types of unaged BBOA (Table 1). The variability in $T_{g,BBOA}$ and κ is likely due to differences in experimental conditions used to generate and sample the BBOA, such as the fuel type, combustion conditions, and dilution. Here we calculated the viscosity of unaged BBOA using each of the $T_{g,BBOA}$ and κ pairs shown in Table 1 to determine the possible range of viscosities and phase states of unaged BBOA in the stratosphere.

The viscosity was calculated from $T_{g,BBOA}$ and κ using the same approach used by Li et al. to calculate viscosity of SOA in the troposphere.[37] First, we calculated the water content of the BBOA at a given RH using κ and the following equations:[26]

$$w_{BBOA} = \frac{\rho_{BBOA}\left(1 - \frac{RH}{100}\right)}{\frac{RH}{100}\left(\frac{\rho_{BBOA}}{\frac{RH}{100}} - \rho_{BBOA} + \kappa\rho_w\right)}, \quad (5)$$

https://doi.org/10.26434/chemrxiv-2024-27934-v4 ORCID: https://orcid.org/0000-0002-5621-2323 Content not peer-reviewed by ChemRxiv. License: CC BY 4.0

and

$$w_{H2O} = 1 - w_{BBOA}, \quad \textbf{(6)}$$

where w_{BBOA} *and* w_{H2O} represent the mass fraction of BBOA and H_2O in a BBOA-water mixture, respectively. In Equation 5, ρ_w represents the density of water, and ρ_{BBOA} represents the density of BBOA. For ρ_w, we used 1 g/cm^3, and for ρ_{BBOA}, we used 1.3 g/cm^3, consistent with previous assumptions and measurements.[38,39]

Subsequently, the glass transition temperature of the BBOA and water mixture ($T_{g,mix}$) was calculated using the Gordon-Taylor equation and the glass transition temperature of dry BBOA ($T_{g,BBOA}$):[18]

$$T_{g,mix}(w_{BBOA}) = \frac{(1-w_{BBOA})T_{g,w} + \frac{w_{BBOA}\,T_{g,BBOA}}{k_{GT}}}{(1-w_{BBOA}) + \frac{w_{BBOA}}{k_{GT}}}, \quad \textit{(7)}$$

where k_{GT} represents the Gordon-Taylor constant, suggested to be 2.5,[18,40,41] and $T_{g,w}$ is the glass transition temperature of water, set to 136 K.[42]

Viscosity at a given temperature (T) was then calculated using the Vogel–Fulcher–Tammann (VFT) equation:[43]

$$\eta = \eta_\infty \exp\left(\frac{T_0\,D}{T - T_0}\right), \quad \textbf{(8)}$$

where η_∞ is the viscosity at infinite temperature (set to 10^{-5} Pa s),[43] D is the fragility parameter, assumed to be 10 as done previously,[24] and T_0 is the Vogel temperature calculated using the following equation:

$$T_0 = \frac{39.17 \cdot T_{g,mix}(w_{BBOA})}{D + 39.17}, \quad \textit{(9)}$$

2.4 Viscosity of aged BBOA-H_2SO_4 particles

To calculate the viscosity of aged BBOA-H_2SO_4 particles at a given RH and temperature, we first determined the viscosity of aged BBOA particles and H_2SO_4 particles separately at the given RH and temperature, as outlined below.

To determine the viscosity of aged BBOA particles at a given RH and temperature, we followed the same method described in Section 2.3. The viscosities determined in Section 2.3 correspond to unaged BBOA. We assume that these viscosities represent lower limits for aged BBOA due to the following factors: a) aging through OH and O_3 reactions has been shown to increase BBOA

https://doi.org/10.26434/chemrxiv-2024-27934-v4 ORCID: https://orcid.org/0000-0002-5621-2323 Content not peer-reviewed by ChemRxiv. License: CC BY 4.0

viscosity at room temperature and on the timescale of days,[23,44] b) UV exposure at room temperature also increases BBOA viscosity on the timescale of days,[45] and c) dilution also increases BBOA viscosity.[46] Nevertheless, additional measurements are needed to confirm this assumption for stratospheric temperatures, relative humidities, and residence times. We hope our work will motivate further studies on this topic. In addition, it is important to keep in mind that unaged BBOA in the stratosphere will often be in a glassy state (see below), and hence aging reactions with OH and O_3 should be limited for initial conditions in the stratosphere.

To determine the viscosity of H_2SO_4 particles at a given RH and temperature, we used the AIOMFAC-VISC thermodynamic model.[47,48] This model applies a semi-empirical approach based on the Eyring's absolute rate theory to describe the viscosity of aqueous electrolyte solutions. The model reproduces viscosity data often within 10% for a wide range of aqueous electrolyte systems.[48]

After determining the viscosity of the aged BBOA particles and H_2SO_4 particles separately at a given RH and temperature, we used the Zdanovskii-Stokes-Robinson (ZSR) approach to calculate the viscosity of aged BBOA-H_2SO_4 particles at the given RH and temperature.[48] The ZSR approach is expressed mathematically as the following:

$$\ln(\eta/\eta^0) = f_1 \ln(\eta_1/\eta^0) + f_2 \ln(\eta_2/\eta^0)\,, \qquad \textbf{(10)}$$

Where η, η_1, and η_2 represents the viscosity of the BBOA-H_2SO_4 particles, BBOA particles, and H_2SO_4 particles, respectively, all at the same RH and temperature. η^0 is the unit viscosity (1 Pa s); and f_1 and f_2 are the mass fractions of the two subsystems at the given RH and temperature. Studies by Song et al.[49] and Klein et al.[28] show that the ZSR approach predicts viscosities within 1 — 2 orders of magnitude for mixtures of organic and inorganic material.

To predict the viscosity of the aged BBOA-H_2SO_4 particles using Equation 10, the H_2SO_4-to-BBOA (H_2SO_4:BBOA) mass ratio is needed. An upper limit to the H_2SO_4:BBOA mass ratio for pyroCb smoke in the stratosphere can be estimated based on limited measurements. In 2017, the NASA Atmospheric Tomography (ATom) mission sampled pryoCb smoke in the northern hemisphere and lowest part of the stratosphere from the large-scale wildfires in the Pacific Northwest of North America.[50,51] Single particle measurements from this mission indicate that the average H_2SO_4:BBOA mass ratio was ~0.37 and ~0.79 for 2 months and 9 months, respectively, after the initial pryoCb injection into the stratosphere (Section S1 and Fig. S2).[50–52] The H_2SO_4:BBOA mass ratio was even smaller for the largest particles ($\gtrsim$ 0.5 μm) (Fig. S2). Based on the size distributions of the typical smoke in the stratosphere and smoke from pryoCb events, the largest particles were likely mostly from pyroCb events, whereas the smaller particles were likely aged smoke that is widespread in the upper troposphere and lower stratosphere.[4,51] Based on these limited measurements, we suggest that H_2SO_4:BBOA mass ratios of 0.37 and 0.79 are likely an upper limit for pyroCb smoke in the lower stratosphere with an aging time of 2 months and 9 months, respectively. To be consistent with the ATom measurements, in the following, we consider H_2SO_4:BBOA mass ratios of 0.37, 0.5, and 0.79.

3. Results and discussion:

https://doi.org/10.26434/chemrxiv-2024-27934-v4 ORCID: https://orcid.org/0000-0002-5621-2323 Content not peer-reviewed by ChemRxiv. License: CC BY 4.0

3.1 RH in the stratosphere

Before discussing the viscosity of BBOA in the stratosphere, we first considered the RH in the stratosphere since the RH strongly impacts particle viscosity. As the RH decreases, the water activity (and hence water content) of BBOA particles decreases to maintain equilibrium with the gas phase and the viscosity increases due to the plasticizing effect of water.[18,53]

We calculated the RH as a function of temperature in the stratosphere at altitudes of 15 and 32 km and a water vapor mixing ratio of 15 ppmv. An altitude range of 15 — 32 km corresponds to the range of altitudes where wildfire plumes have been observed in the stratosphere.[29–31] A water vapor mixing ratio of 15 ppmv is consistent with the water vapour mixing ratio expected in wildfire plumes that have reached the stratosphere via pryoCb events.[29 35]

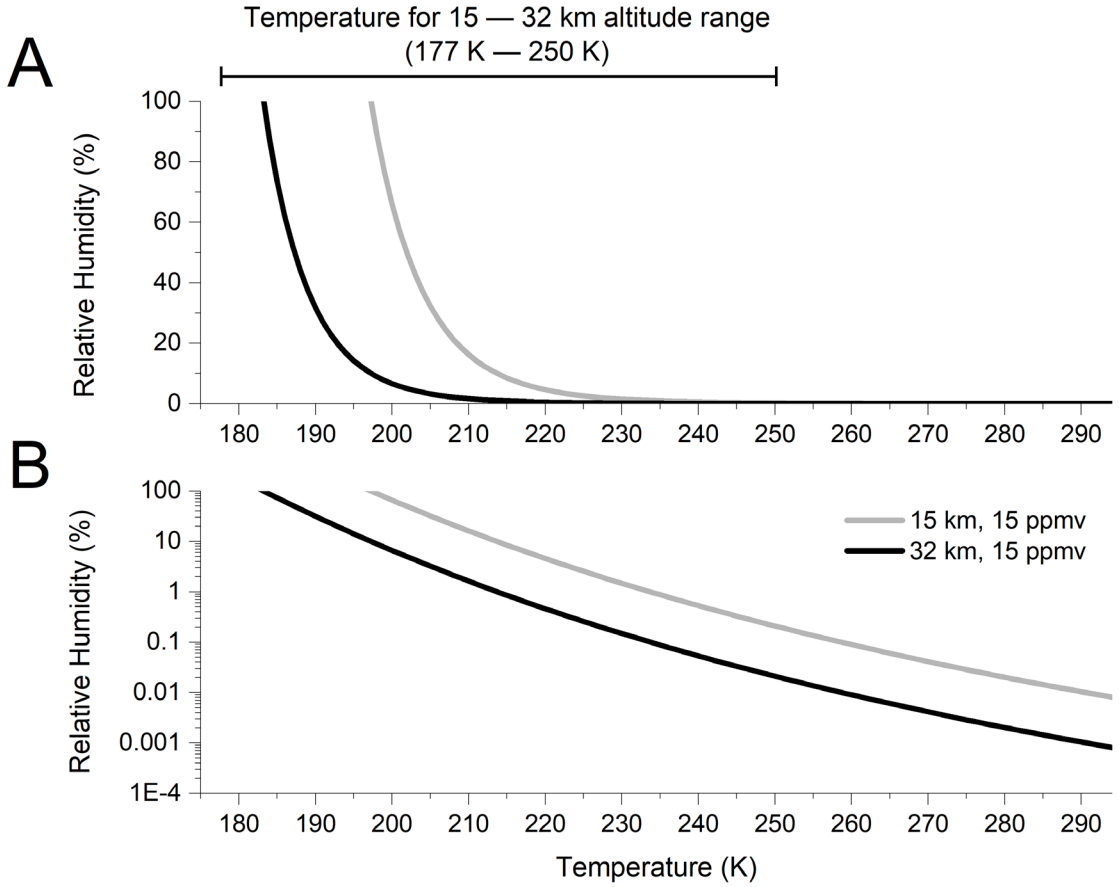

Figure 2. *RH as a function of temperature in the stratosphere for altitudes of 15 and 32 km and a water vapor mixing ratio of 15 ppmv. (A) Data with the RH on a linear scale, and (B) data with the RH on a logarithmic scale.*

The results of the calculations are shown in Figure 2. The horizontal bar illustrates the temperature range of 177 — 250 K, which is most relevant for the BBOA in the stratosphere from pyroCb events at altitudes of 15 — 32 km (see Methods). Our calculations indicate that the

https://doi.org/10.26434/chemrxiv-2024-27934-v4 **ORCID:** https://orcid.org/0000-0002-5621-2323 Content not peer-reviewed by ChemRxiv. **License:** CC BY 4.0

RH reaches extremely low levels ($\lesssim$ 1% RH) under a wide range of conditions relevant to BBOA in the stratosphere. In contrast, in the troposphere, the RH is almost always greater than 10%.[54] The low RH levels relevant for BBOA in the stratosphere, combined with the cold stratospheric temperatures, have significant implications for the viscosity of BBOA in this region as discussed below.

3.2 The viscosity of unaged BBOA in the stratosphere

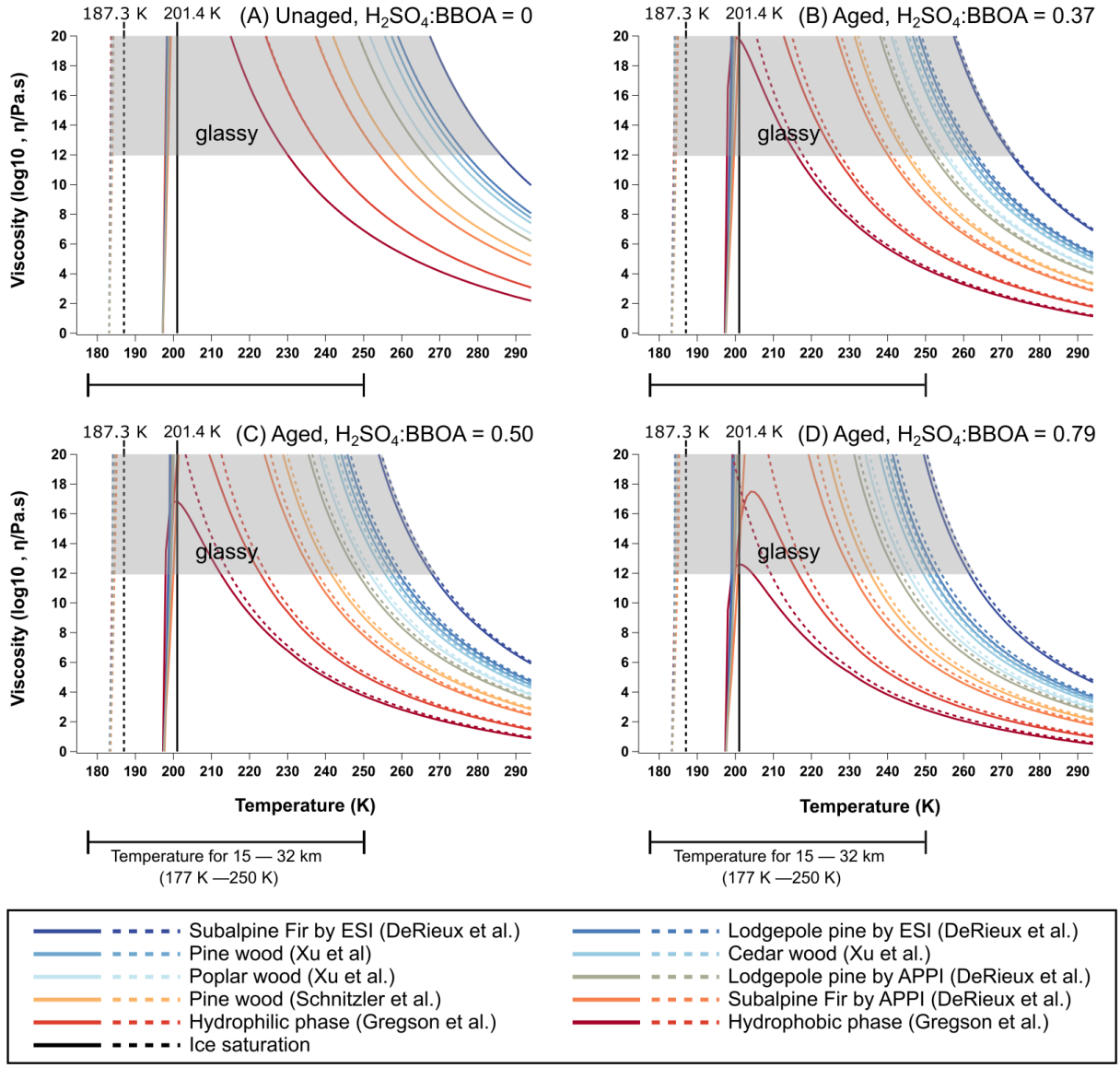

Figure 3. *The viscosity of different BBOA types mixed with H_2SO_4 as a function of the temperature in the stratosphere (coloured lines). Also superimposed are the ice saturation conditions (black lines). Grey regions represent conditions where BBOA-H_2SO_4 mixtures are glassy (viscosity $\geq 10^{12}$ Pa s). Calculations were done using a fragility parameter of D=10, at a water pressure of 15 ppmv, and at altitudes of 15 km (solid lines) and 32 km (dashed lines). Viscosities extended beyond 10^{20} Pa s, however the y-axis was capped at this value.*

https://doi.org/10.26434/chemrxiv-2024-27934-v4 **ORCID:** https://orcid.org/0000-0002-5621-2323 Content not peer-reviewed by ChemRxiv. **License:** CC BY 4.0

Shown in Figure 3A are the calculated viscosities for the 10 unaged BBOA types listed in Table 1. Similar to Figure 2, we carried out calculations for the stratosphere at altitudes of 15 and 32 km and a water vapour mixing ratio of 15 ppmv. For the temperature range of 200 — 250 K, all the BBOA types have viscosities of approximately 10^7 Pa s or greater (Fig. 3A). These extremely high viscosities are due to a combination of low RH values and low temperatures (Fig 2). Furthermore, 8 out of the 10 BBOA types exhibit viscosities exceeding 10^{12} Pa s for the entire temperature range of 200 —250 K, indicating that they are predicted to remain in a glassy solid state throughout this range. For the 2 proxies studied by Gregson et al. a glassy solid state was observed over a narrower range of temperatures (200 — 230 K for the hydrophobic phase and 200 — 240 K for hydrophilic phase), but the glassy state still dominated between 200 — 250 K. Overall, these results suggest that the glass state dominates for unaged BBOA in the stratosphere for the 200 — 250 K temperature range. At temperatures $\lesssim$ 200 K all of the BBOA types switch from a glassy solid state to a semisolid or liquid state (Fig. 3A) due to the heightened RH in this low-temperature regime (Figure 2). At an altitude of 15 km, the transition from a glassy state to a semisolid/liquid state occurs at about 195 — 200 K. At an altitude of 32 km, the transition occurs at about 180 — 185 K.

3.3 Viscosity of aged BBOA-H_2SO_4 particles

Figure 3 also includes calculated viscosities for aged BBOA-H_2SO_4 particles with with H_2SO_4:BBOA mass ratios of 0.37, 0.5, and 0.79. Measurements from the ATom mission suggest that H_2SO_4:BBOA mass ratios of 0.37 and 0.79 are likely upper limit for pyroCb smoke in the lower stratosphere with aging times of 2 months and 9 months, respectively (see Methods). The H_2SO_4:BBOA mass ratio of 0.5 is provided as an intermediate value between the ratios of 0.37 and 0.79.

To calculate the viscosities of aged BBOA-H_2SO_4 particles, we used the viscosities of unaged BBOA as proxies for aged BBOA. Consequently, the calculated viscosities should be considered as lower limits to the viscosities of aged BBOA-H_2SO_4 particles for several reasons that are outlined in the Methods section.

For H_2SO_4:BBOA = 0.37 (Fig. 3B) at temperatures between 200 — 250 K, the viscosity of the aged BBOA- H_2SO_4 particles is approximately 3 orders of magnitude lower, or more, compared to the unaged case (compare Fig. 3A and 3B). This decrease is attributed to the low viscosity of the H_2SO_4 and its associated water compared to BBOA at the same RH and temperature. Despite the reduction in viscosity, for the temperature range of 200 — 250 K, all the BBOA types have viscosities of approximately 10^4 Pa s or greater. In addition, 6 out of the 10 systems still exhibited viscosities greater than 10^{12} Pa s for the full temperature range of 200 — 250 K. For the remaining 4 systems, the particles still reached 10^{12} Pa s, although over a narrower temperature range. Overall, these results suggest that aged BBOA with a H_2SO_4:BBOA mass ratio of 0.37 will have a viscosity of approximately 10^4 Pa or greater and will often be in a glassy state for the temperature range of 200 — 250K.

For H_2SO_4:BBOA = 0.37 (Fig. 3B) at temperatures $\lesssim$ 200 K, all of the aged BBOA-H_2SO_4 types transition from a glassy solid state to a semisolid or liquid state due to the increased RH in this

https://doi.org/10.26434/chemrxiv-2024-27934-v4 ORCID: https://orcid.org/0000-0002-5621-2323 Content not peer-reviewed by ChemRxiv. License: CC BY 4.0

low-temperature regime. At an altitude of 15 km, the transition from a glassy state to a semisolid/liquid state occurs at about 195 — 200 K, while at an altitude of 32 km, the transition occurs at about 180 — 185 K.

For H_2SO_4:BBOA = 0.79 (Fig.3D) at temperatures between 200 and 250 K, the viscosity decreases by 1 order of magnitude, or more, compared to H_2SO_4:BBOA = 0.37. Again, this reduction is attributed to the low viscosity of the H_2SO_4 and its associated RH compared to BBOA at the same RH and temperature. For the temperature range of 200 — 250 K, all the BBOA types have viscosities of approximately 10^3 Pa s or greater. In addition, 3 out of the 10 systems exhibited viscosities greater than 10^{12} Pa s for the full temperature range of 200 — 250 K. For the remaining 7 systems, the particles still reach 10^{12} Pa s, although over a more narrow temperature range. Overall, these results suggest that aged BBOA with a H_2SO_4:BBOA mass ratio 0.79 will have viscosities of approximately 10^3 Pa s or greater for the temperature range of 200 to 250 K. In addition, the glass state will form in these aged BBOA for some stratospheric conditions.

3.4 Sensitivity analysis

In the analysis above, we used a C_{H2O} value of 15 ppmv, consistent with measurements in plumes that recently entered the stratosphere via pyroCb events. Over time, C_{H2O} levels decrease due to dilution, eventually reaching background values of ~5 ppmv. To evaluate how a reduction in C_{H2O} affects viscosity and phase state, we recalculated viscosities using a C_{H2O} value of 5 ppmv (Figure S4). The lower C_{H2O} level increases viscosity. For example, for the hydrophobic phase studied by Gregson et al., H_2SO_4:BBOA =0.79, C_{H2O} = 15 ppmv, and an altitude of 15 km, the highest observed viscosity was ~10^{12} Pa s. In contrast, under the same conditions but with C_{H2O} = 5 ppmv, the highest observed viscosity was ~10^{22} Pa s.

To calculate the viscosities of aged BBOA-H_2SO_4 particles, we used the ZSR method. Previous studies have demonstrated that the ZSR method can estimate the viscosity of mixed organic and inorganic particles within 1 — 2 orders of magnitude.[28,49] Figure S5 presents the predicted viscosities of aged BBOA-H_2SO_4 particles (C_{H2O} = 15 ppmv and H_2SO_4:BBOA ratio = 0.37, 0.5, and 0.79) with all of the predicted viscosities reduced by two orders of magnitude. Even after this reduction, the aged BBOA with a H_2SO_4:BBOA mass ratio of 0.37 are still predicted to be in a glassy state often for the 200 — 250 K temperature range. In addition, the aged BBOA with a H_2SO_4:BBOA mass ratio of 0.79 will still form the glass state for some stratospheric conditions and BBOA types.

To calculate the viscosity of BBOA particles from their glass transition temperatures, we assumed a fragility parameter (D) of 10, consistent with values used in previous studies. For individual organic molecules, D values typically range from 5 to 20. To assess the impact of this range, we recalculated viscosities using D values of 5 and 20, with a water vapour mixing ratios of 15 ppmv and H_2SO_4:BBOA mass ratios of 0, 0.37, 0.5, and 0.79 (Figure S6 and S7). The largest reductions in viscosity were observed for a D value of 20. Nevertheless, even for D = 20, the aged BBOA with a H_2SO_4:BBOA mass ratio of 0.37 are still predicted to be in a glassy state often for the 200 — 250 K temperature range. In addition, the aged BBOA with a H_2SO_4:BBOA

https://doi.org/10.26434/chemrxiv-2024-27934-v4 ORCID: https://orcid.org/0000-0002-5621-2323 Content not peer-reviewed by ChemRxiv. License: CC BY 4.0

mass ratio of 0.79 are still predicted to form the glass state for some stratospheric conditions and BBOA types.

4. Atmospheric Implications

Recent studies have suggested that reactions occur on or in BBOA in the stratosphere, leading to unexpected depletion of the UV-blocking stratospheric ozone layer.[13–15] In modelling studies, researchers have assumed that the BBOA-H_2SO_4 particles in the stratosphere are in a non-glassy state and that reactions occur in the bulk of the BBOA-H_2SO_4 particles.[14,15] These assumptions have generally aligned with model-measurement comparisons. Our results suggest that wildfire smoke particles will have viscosities $\gtrsim 10^3$ Pa s, when the H_2SO_4:BBOA mass ratio is $\lesssim 0.79$ and the temperature is 200 — 250 K. These high viscosities can influence the characteristic reaction diffusive length scale and reactive uptake rates. For instance, reactive uptake rates often scale with the square root of 1/viscosity, meaning a two-order-of-magnitude increase in viscosity can reduce the reactive uptake rate by one order of magnitude.[16] Consequently, these elevated viscosities may need to be considered to accurately describe the stratospheric chemistry of wildfire smoke particles.

Our results also suggest that wildfire smoke particles can be in a glassy state (viscosity $\geq 10^{12}$ Pa s) under certain temperatures and RHs in the stratosphere when the H_2SO_4:BBOA mass ratio is $\lesssim 0.79$. In such a state, bulk reactions will be inhibited, and multiphase chemistry may be restricted to the surface of the particles. Therefore, surface reactions may need to be considered for some conditions in the stratosphere.

As mentioned above, BBOA may influence the formation mechanisms of PSCs via several pathways (Fig. 1B). In the current study, we address the possibility of pathway c in Figure 1B. In Figure 3, we show the RH and temperature conditions where vapor becomes supersaturated with respect to ice, indicated by vertical black lines. The solid black line corresponds to conditions at an altitude of 15 km, while the dashed black line corresponds to an altitude of 32 km. If viscosity is $\geq 10^{12}$ Pa s to the left of the vertical black lines (i.e., colder temperatures) at the respective altitudes, BBOA can exist in a glassy state while the vapor is supersaturated with respect to ice. This glassy state may provide a surface for heterogeneous ice nucleation, leading to the formation of ice-containing PSCs (pathway c, Fig. 1B).

For H_2SO_4:BBOA ratios of 0, 0.37, 0.5, and 0.79 at altitudes of 15 km and 32 km (Fig. 3), the viscosity is $\geq 10^{12}$ Pa s to the left of the corresponding vertical black lines. This indicates that under certain stratospheric conditions, the particles are in a glassy state, the vapor is supersaturated with respect to ice, and the particles can act as potential surfaces for heterogeneous ice nucleation, possibly leading to the formation of ice-containing PSCs (pathway c, Fig. 1B).

Lidar observations indicate that fresh smoke particles in the stratosphere exhibit a high depolarization ratio, suggesting the presence of non-spherical particles.[1,55–57] This elevated depolarization could signal that BBOA is in a glassy or highly viscous state in the stratosphere. In newly emitted smoke plumes, BBOA particles can coagulate into fractal aggregates.[58] If

https://doi.org/10.26434/chemrxiv-2024-27934-v4 ORCID: https://orcid.org/0000-0002-5621-2323 Content not peer-reviewed by ChemRxiv. License: CC BY 4.0

BBOA is in a glassy or highly viscous state, the material will not flow, maintaining its fractal structure after coagulation, which would contribute to a high depolarization ratio.[59–61] Additionally, black carbon particles from combustion sources initially have a fractal geometry. When coated with a low-viscosity material, the fractal geometry can become more compact and spherical, with a low depolarization ratio.[62] However, if black carbon is coated with BBOA in a glassy or highly viscous state, black carbon can maintain its fractal geometry, and the depolarization ratio can stay high.[62] Nevertheless, interpretation of lidar depolarization is complicated because depolarization depends on particle size as well as the degree of non-sphericity.[59]

Lidar data also show that the depolarization ratio of smoke in the stratosphere decreases over a period of 3 — 4 months, eventually approaching near-zero values (< 0.05).[1,63] This trend may indicate that BBOA transition from a highly viscous state to a less viscous one. A decrease in viscosity would allow fractal aggregates of BBOA to transform into spherical particles, which typically exhibit a near-zero depolarization ratio. Similarly, a reduction in BBOA viscosity would enable fractal black carbon aggregates coated with BBOA to compact into a core-shell structure, also associated with a low depolarization ratio. However, it is important to note that glassy or highly viscous BBOA, such as tar balls, that have not coagulated into fractal aggregates in the atmosphere will possess a spherical geometry and exhibit a low depolarization ratio.[64,65] Therefore, a low depolarization ratio does not definitively indicate that BBOA particles are in a non-glassy and non-viscous state.

Baars et al. pointed out that the decrease in depolarization ratio of smoke in the stratosphere with time is consistent with the aging of smoke particles and the addition of a coating around the solid black carbon core aggregates, which would change the shape towards a spherical form.[1] We add here that the coating would also need to be in a non-glassy and lower viscosity state,[62] which may be accomplished by the uptake of H_2SO_4 present in the stratosphere, as shown above.

5. Outlook

1) When calculating the viscosity of aged BBOA-H_2SO_4 particles, we assumed the viscosity of unaged BBOA is a lower limit to the viscosity of aged BBOA for several reasons (see Methods). Nevertheless, additional measurements are needed to confirm this assumption for stratospheric temperatures, relative humidities, and residence times.
2) We assumed that BBOA forms a single phase when mixed with H_2SO_4. Previous studies have shown that when secondary organic aerosol with an average O/C ratio $\gtrsim 0.8$ is mixed with ammonium sulfate aerosols, the resulting particles form a single phase.[66–68] Studies are needed to confirm if a similar threshold applies for BBOA mixed with H_2SO_4.
3) To calculate the viscosity of BBOA particles from their glass transition temperatures, we assumed a fragility parameter (D) of 10, consistent with values used in previous studies. Measurements are needed to confirm that a fragility of 10 is appropriate for BBOA.
4) To calculate the viscosity of aged BBOA-H_2SO_4 particles, we used the ZSR method and the AIOMFAC-VISC thermodynamic model. Observations are needed to confirm the validity of this approach specifically for laboratory-generated and field-collected BBOA-H_2SO_4 particles.

https://doi.org/10.26434/chemrxiv-2024-27934-v4 **ORCID:** https://orcid.org/0000-0002-5621-2323 Content not peer-reviewed by ChemRxiv. **License:** CC BY 4.0

5) More measurements of the H_2SO_4 content in wildfire aerosols as a function of age in the stratosphere are needed. These measurements could be carried out by high-altitude aircraft or by using infrared spectra of wildfire smoke in the stratosphere from satellite measurements.[13]

6) Additional observational constraints on the viscosity and phase state of BBOA in the stratosphere are needed. Lidar depolarization measurements of wildfire smoke in the stratosphere offer valuable insights into these properties, but additional measurements are needed. Lidar depolarization measurements indicate that wildfire smoke in the stratosphere is often non-spherical,[63] but depolarization is an indirect measurement that does not uniquely determine phase and viscosity.

7) Measurements should also differentiate between ordinary smoke particles slowly lofted into the stratosphere and smoke rapidly injected into the stratosphere through large pyroCb events. PyroCb smoke is processed through a cloud during its ascent. This could result in a different mix of organic molecules than smoke that is not cloud-processed.

8) Our results suggest that aged BBOA and aged BBOA mixed with H_2SO_4 will be in a glassy state for some conditions in the stratosphere. Previous studies have shown that certain types of organic aerosols in a glassy state can nucleate ice heterogeneously.[69–72] However, the ice nucleation efficiency of glassy organic aerosols is still an area of active research.[73] Studies are needed to determine whether BBOA in a glassy state can nucleate crystalline PSCs.

9) We considered the uptake of water and H_2SO_4 by BBOA in the stratosphere. At the coldest temperatures, BBOA particles can also take up nitric acid (HNO_3), similar to background H_2SO_4 particles in the stratosphere, which could further change the composition, and hence, the viscosity of the wildfire smoke particles.[74] Smoke particles can also take up HCl and potentially other chlorine compounds.[15] This uptake should be considered in future studies.

Author contributions:

The writing of the manuscript was led by AKB with contributions from MFZ. MFZ calculated viscosities from glass transition temperatures of BBOA and produced the figures in the manuscript with contributions from NGG. AZ calculated the viscosities of sulfuric acid particles using the AIOMFAC-VISC thermodynamic model and provided direction and insight for viscosity predictions. DM and GS provided measurements of BBOA in the lower stratosphere. DM identified the observational constraints of viscosity and phase state in the stratosphere. All authors discussed and interpreted data and contributed to revising the original manuscript.

Supporting Information

Details of the ATom campaign, H_2SO_4:BBOA mass ratio figure, simulated monthly temperature figure, and BBOA viscosity figures for sensitivity analyses (DOC).

Acknowledgements:

The authors thank Yifeng Peng from Lanzhou University for providing simulated zonal mean monthly temperatures from the Whole Atmosphere Community Climate Model (WACCM).

Financial support:

https://doi.org/10.26434/chemrxiv-2024-27934-v4 **ORCID:** https://orcid.org/0000-0002-5621-2323 Content not peer-reviewed by ChemRxiv. **License:** CC BY 4.0

This research has been supported by the Natural Sciences and Engineering Research Council of Canada (grant no. RGPIN-2023-05333 and RGPIN-2021-02688) and Environment and Climate Change Canada (grant no. GCXE20S049). We also acknowledge support from the Natural Sciences and Engineering Research Council of Canada for a postgraduate scholarship award (PGS D-579464-2023) for funding NGAG. The ATom mission as a whole was supported by NASA's Earth System Science Pathfinder Program EVS-2 funding. Participation in ATom Mission flights by DMM and GPS was supported by NOAA climate funding (no. NNH15AB12I).

References:

(1) Baars, H.; Ansmann, A.; Ohneiser, K.; Haarig, M.; Engelmann, R.; Althausen, D.; Hanssen, I.; Gausa, M.; Pietruczuk, A.; Szkop, A.; Stachlewska, I. S.; Wang, D. X.; Reichardt, J.; Skupin, A.; Mattis, I.; Trickl, T.; Vogelmann, H.; Navas-Guzman, F.; Haefele, A.; Acheson, K.; Ruth, A. A.; Tatarov, B.; Muller, D.; Hu, Q. Y.; Podvin, T.; Goloub, P.; Veselovskii, I.; Pietras, C.; Haeffelin, M.; Freville, P.; Sicard, M.; Comeron, A.; Garcia, A. J. F.; Menendez, F. M.; Cordoba-Jabonero, C.; Guerrero-Rascado, J. L.; Alados-Arboledas, L.; Bortoli, D.; Costa, M. J.; Dionisi, D.; Liberti, G. L.; Wang, X.; Sannino, A.; Papagiannopoulos, N.; Boselli, A.; Mona, L.; D'Amico, G.; Romano, S.; Perrone, M. R.; Belegante, L.; Nicolae, D.; Grigorov, I.; Gialitaki, A.; Amiridis, V.; Soupiona, O.; Papayannis, A.; Mamouri, R. E.; Nisantzi, A.; Heese, B.; Hofer, J.; Schechner, Y. Y.; Wandinger, U.; Pappalardo, G. The Unprecedented 2017-2018 Stratospheric Smoke Event: Decay Phase and Aerosol Properties Observed with the EARLINET. *Atmos. Chem. Phys.* **2019**, *19* (23), 15183–15198. https://doi.org/10.5194/acp-19-15183-2019.

(2) Peterson, D. A.; Fromm, M. D.; McRae, R. H. D.; Campbell, J. R.; Hyer, E. J.; Taha, G.; Camacho, C. P.; Kablick, G. P.; Schmidt, C. C.; DeLand, M. T. Australia's Black Summer Pyrocumulonimbus Super Outbreak Reveals Potential for Increasingly Extreme Stratospheric Smoke Events. *Npj Clim. Atmos. Sci.* **2021**, *4* (38), 1–16. https://doi.org/10.1038/s41612-021-00192-9.

(3) Schill, G. P.; Froyd, K. D.; Bian, H.; Kupc, A.; Williamson, C.; Brock, C. A.; Ray, E.; Hornbrook, R. S.; Hills, A. J.; Apel, E. C.; Chin, M.; Colarco, P. R.; Murphy, D. M. Widespread Biomass Burning Smoke throughout the Remote Troposphere. *Nat. Geosci.* **2020**, *13* (6), 422–427. https://doi.org/10.1038/s41561-020-0586-1.

(4) Murphy, D. M.; Froyd, K. D.; Bourgeois, I.; Brock, C. A.; Kupc, A.; Peischl, J.; Schill, G. P.; Thompson, C. R.; Williamson, C. J.; Yu, P. Radiative and Chemical Implications of the Size and Composition of Aerosol Particles in the Existing or Modified Global Stratosphere. *Atmos. Chem. Phys.* **2021**, *21* (11), 8915–8932. https://doi.org/10.5194/acp-21-8915-2021.

(5) Reid, J. S.; Koppmann, R.; Eck, T. F.; Eleuterio, D. P. A Review of Biomass Burning Emissions Part II: Intensive Physical Properties of Biomass Burning Particles. *Atmos. Chem. Phys.* **2005**, *5*, 799–825. https://doi.org/10.5194/acp-5-799-2005.

(6) Liu, X.; Huey, L. G.; Yokelson, R. J.; Selimovic, V.; Simpson, I. J.; Müller, M.; Jimenez, J. L.; Campuzano-Jost, P.; Beyersdorf, A. J.; Blake, D. R.; Butterfield, Z.; Choi, Y.; Crounse, J. D.; Day, D. A.; Diskin, G. S.; Dubey, M. K.; Fortner, E.; Hanisco, T. F.; Hu,

https://doi.org/10.26434/chemrxiv-2024-27934-v4 **ORCID:** https://orcid.org/0000-0002-5621-2323 Content not peer-reviewed by ChemRxiv. **License:** CC BY 4.0

W.; King, L. E.; Kleinman, L.; Meinardi, S.; Mikoviny, T.; Onasch, T. B.; Palm, B. B.; Peischl, J.; Pollack, I. B.; Ryerson, T. B.; Sachse, G. W.; Sedlacek, A. J.; Shilling, J. E.; Springston, S.; St. Clair, J. M.; Tanner, D. J.; Teng, A. P.; Wennberg, P. O.; Wisthaler, A.; Wolfe, G. M. Airborne Measurements of Western U.S. Wildfire Emissions: Comparison with Prescribed Burning and Air Quality Implications. *J. Geophys. Res.* **2017**, *122* (11), 6108–6129. https://doi.org/10.1002/2016JD026315.

(7) May, A. A.; McMeeking, G. R.; Lee, T.; Taylor, J. W.; Craven, J. S.; Burling, I.; Sullivan, A. P.; Akagi, S.; Collett Jr., J. L.; Flynn5, H. C.; Urbanski, S. P.; Seinfeld, J. H.; Yokelson, R. J.; Kreidenweis, S. M. Aerosol Emissions from Prescribed Fires in the United States: A Synthesis of Laboratory and Aircraft Measurements. *J. Geophys. Res.* **2014**, *119* (20), 11826–11849. https://doi.org/10.1002/ 2014JD021848.

(8) Hodshire, A. L.; Akherati, A.; Alvarado, M. J.; Brown-Steiner, B.; Jathar, S. H.; Jimenez, J. L.; Kreidenweis, S. M.; Lonsdale, C. R.; Onasch, T. B.; Ortega, A. M.; Pierce, J. R. Aging Effects on Biomass Burning Aerosol Mass and Composition: A Critical Review of Field and Laboratory Studies. *Environ. Sci. Technol.* **2019**, *53* (17), 10007–10022. https://doi.org/10.1021/acs.est.9b02588.

(9) Rickly, P. S.; Guo, H.; Campuzano-Jost, P.; Jimenez, J. L.; Wolfe, G. M.; Bennett, R.; Bourgeois, I.; Crounse, J. D.; Dibb, J. E.; Digangi, J. P.; Diskin, G. S.; Dollner, M.; Gargulinski, E. M.; Hall, S. R.; Halliday, H. S.; Hanisco, T. F.; Hannun, R. A.; Liao, J.; Moore, R.; Nault, B. A.; Nowak, J. B.; Peischl, J.; Robinson, C. E.; Ryerson, T.; Sanchez, K. J.; Schöberl, M.; Soja, A. J.; St. Clair, J. M.; Thornhill, K. L.; Ullmann, K.; Wennberg, P. O.; Weinzierl, B.; Wiggins, E. B.; Winstead, E. L.; Rollins, A. W. Emission Factors and Evolution of SO_2 Measured from Biomass Burning in Wildfires and Agricultural Fires. *Atmos. Chem. Phys.* **2022**, *22* (23), 15603–15620. https://doi.org/10.5194/acp-22-15603-2022.

(10) Andreae, M. O. Emission of Trace Gases and Aerosols from Biomass Burning - an Updated Assessment. *Atmos. Chem. Phys.* **2019**, *19* (13), 8523–8546. https://doi.org/10.5194/acp-19-8523-2019.

(11) Kettle, A. J.; Kuhn, U.; Von Hobe, M.; Kesselmeier, J.; Andreae, M. O. Global Budget of Atmospheric Carbonyl Sulfide: Temporal and Spatial Variations of the Dominant Sources and Sinks. *J. Geophys. Res. Atmos.* **2002**, *107* (22), 1–16. https://doi.org/10.1029/2002JD002187.

(12) Höpfner, M.; Boone, C. D.; Funke, B.; Glatthor, N.; Grabowski, U.; Günther, A.; Kellmann, S.; Kiefer, M.; Linden, A.; Lossow, S.; Pumphrey, H. C.; Read, W. G.; Roiger, A.; Stiller, G.; Schlager, H.; Von Clarmann, T.; Wissmüller, K. Sulfur Dioxide (SO_2) from MIPAS in the Upper Troposphere and Lower Stratosphere 2002-2012. *Atmos. Chem. Phys.* **2015**, *15* (12), 7017–7037. https://doi.org/10.5194/acp-15-7017-2015.

(13) Bernath, P.; Boone, C.; Crouse, J. Wildfire Smoke Destroys Stratospheric Ozone. *Science* **2022**, *375* (6586), 1292–1295. https://doi.org/10.1126/science.abm5611.

(14) Solomon, S.; Dube, K.; Stone, K.; Yu, P.; Kinnison, D.; Toon, O. B.; Strahan, S. E.; Rosenlof, K. H.; Portmann, R.; Davis, S.; Randel, W.; Bernath, P.; Boone, C.; Bardeen, C. G.; Bourassa, A.; Zawada, D.; Degenstein, D. On the Stratospheric Chemistry of Midlatitude Wildfire Smoke. *Proc. Natl. Acad. Sci.* **2022**, *119* (10), 1–9. https://doi.org/10.1073/pnas.2117325119.

(15) Solomon, S.; Stone, K.; Yu, P.; Murphy, D. M.; Kinnison, D.; Ravishankara, A. R.; Wang, P. Chlorine Activation and Enhanced Ozone Depletion Induced by Wildfire Aerosol.

https://doi.org/10.26434/chemrxiv-2024-27934-v4 **ORCID:** https://orcid.org/0000-0002-5621-2323 Content not peer-reviewed by ChemRxiv. **License:** CC BY 4.0

Nature **2023**, *615* (7951), 259–264. https://doi.org/10.1038/s41586-022-05683-0.
(16) Shi, Q.; Jayne, J. T.; Kolb, C. E.; Worsnop, D. R.; Davidovits, P. Kinetic Model for Reaction of $ClONO_2$ with H_2O and HCl and HOCl with HCl in Sulfuric Acid Solutions. *J. Geophys. Res.* **2001**, *106* (D20), 24259–24274. https://doi.org/10.1029/2000jd000181.
(17) Ansmann, A.; Ohneiser, K.; Chudnovsky, A.; Knopf, D. A.; Eloranta, E. W.; Villanueva, D.; Seifert, P.; Radenz, M.; Barja, B.; Zamorano, F.; Jimenez, C.; Engelmann, R.; Baars, H.; Griesche, H.; Hofer, J.; Althausen, D.; Wandinger, U. Ozone Depletion in the Arctic and Antarctic Stratosphere Induced by Wildfire Smoke. *Atmos. Chem. Phys.* **2022**, *22* (17), 11701–11726. https://doi.org/10.5194/acp-22-11701-2022.
(18) Koop, T.; Bookhold, J.; Shiraiwa, M.; Pöschl, U. Glass Transition and Phase State of Organic Compounds: Dependency on Molecular Properties and Implications for Secondary Organic Aerosols in the Atmosphere. *Phys. Chem. Chem. Phys.* **2011**, *13* (43), 19238–19255. https://doi.org/10.1039/c1cp22617g.
(19) Schnitzler, E. G.; Gerrebos, N. G. A.; Carter, T. S.; Huang, Y.; Heald, L.; Bertram, A. K.; Abbatt, J. P. D. Rate of Atmospheric Brown Carbon Whitening Governed by Environmental Conditions. *Proc. Natl. Acad. Sci.* **2022**, *119* (38), 1–7.
(20) Gregson, F. K. A.; Gerrebos, N. G. A.; Schervish, M.; Nikkho, S.; Schnitzler, E. G.; Schwartz, C.; Carlsten, C.; Abbatt, J. P. D.; Kamal, S.; Shiraiwa, M.; Bertram, A. K. Phase Behavior and Viscosity in Biomass Burning Organic Aerosol and Climatic Impacts. *Environ. Sci. Technol.* **2023**, *57* (39), 14548–14557. https://doi.org/10.1021/acs.est.3c03231.
(21) Rasool, Q. Z.; Shrivastava, M.; Liu, Y.; Gaudet, B.; Zhao, B. Modeling the Impact of the Organic Aerosol Phase State on Multiphase OH Reactive Uptake Kinetics and the Resultant Heterogeneous Oxidation Timescale of Organic Aerosol in the Amazon Rainforest. *ACS Earth Sp. Chem.* **2023**, *7* (5), 1009–1024. https://doi.org/10.1021/acsearthspacechem.2c00366.
(22) Li, J.; Forrester, S. M.; Knopf, D. A. Heterogeneous Oxidation of Amorphous Organic Aerosol Surrogates by O_3, NO_3, and OH at Typical Tropospheric Temperatures. *Atmos. Chem. Phys.* **2020**, *20* (10), 6055–6080. https://doi.org/10.5194/acp-20-6055-2020.
(23) Xu, W.; Li, Z.; Zhang, Z.; Li, J.; Karnezi, E.; Lambe, A. T.; Zhou, W.; Sun, J.; Du, A.; Li, Y.; Sun, Y. Changes in Physicochemical Properties of Organic Aerosol during Photochemical Aging of Cooking and Burning Emissions. *J. Geophys. Res.* **2023**, *128* (14), 1–14.
(24) DeRieux, W. S. W.; Li, Y.; Lin, P.; Laskin, J.; Laskin, A.; Bertram, A. K.; Nizkorodov, S. A.; Shiraiwa, M. Predicting the Glass Transition Temperature and Viscosity of Secondary Organic Material Using Molecular Composition. *Atmos. Chem. Phys.* **2018**, *18* (9), 6331–6351. https://doi.org/10.5194/acp-18-6331-2018.
(25) Maclean, A. M.; Li, Y.; Crescenzo, G. V; Smith, N. R.; Karydis, V. A.; Tsimpidi, A. P.; Butenho, C. L.; Faiola, C. L.; Lelieveld, J.; Nizkorodov, S. A.; Shiraiwa, M.; Bertram, A. K. Global Distribution of the Phase State and Mixing Times within 2 Secondary Organic Aerosol Particles in the Troposphere Based on 3 Room-Temperature Viscosity Measurements. *ACS Earth Sp. Chem.* **2021**, *5*, 3458–3473. https://doi.org/10.1021/acsearthspacechem.1c00296.
(26) Shiraiwa, M.; Li, Y.; Tsimpidi, A. P.; Karydis, V. A.; Berkemeier, T.; Pandis, S. N.; Lelieveld, J.; Koop, T.; Pöschl, U. Global Distribution of Particle Phase State in Atmospheric Secondary Organic Aerosols. *Nat. Commun.* **2017**, *8* (15002), 1–7.

https://doi.org/10.26434/chemrxiv-2024-27934-v4 **ORCID:** https://orcid.org/0000-0002-5621-2323 Content not peer-reviewed by ChemRxiv. **License:** CC BY 4.0

https://doi.org/10.1038/ncomms15002.
(27) Li, Y.; Carlton, A. G.; Shiraiwa, M. Diurnal and Seasonal Variations in the Phase State of Secondary Organic Aerosol Material over the Contiguous US Simulated in CMAQ. *ACS Earth Sp. Chem.* **2021**, *5* (8), 1971–1982. https://doi.org/10.1021/acsearthspacechem.1c00094.
(28) Klein, L. K.; Bertram, A. K.; Zuend, A.; Gregson, F.; Krieger, U. K. Viscosity of Aqueous Ammonium Nitrate–Organic Particles: Equilibrium Partitioning May Be a Reasonable Assumption for Most Tropospheric Conditions. *EGUsphere* **2024**, *2024* (24), 13341–13359.
(29) Kablick, G. P.; Allen, D. R.; Fromm, M. D.; Nedoluha, G. E. Australian PyroCb Smoke Generates Synoptic-Scale Stratospheric Anticyclones. *Geophys. Res. Lett.* **2020**, *47* (13), 1–9. https://doi.org/10.1029/2020gl088101.
(30) Lee, H.; Lundquist, K. A.; Tang, Q. Pyrocumulonimbus Events Over British Columbia in 2017: An Ensemble Model Study of Parameter Sensitivities and Climate Impacts of Wildfire Smoke in the Stratosphere. *J. Geophys. Res. Atmos.* **2023**, *128* (2), 1–19. https://doi.org/10.1029/2022jd037648.
(31) Yu, P. F.; Davis, S. M.; Toon, O. B.; Portmann, R. W.; Bardeen, C. G.; Barnes, J. E.; Telg, H.; Maloney, C.; Rosenlof, K. H. Persistent Stratospheric Warming Due to 2019-2020 Australian Wildfire Smoke. *Geophys. Res. Lett.* **2021**, *48* (7), 1–9. https://doi.org/10.1029/2021gl092609.
(32) Hurrell, J. W.; Holland, M. M.; Gent, P. R.; Ghan, S.; Kay, J. E.; Kushner, P. J.; Lamarque, J. F.; Large, W. G.; Lawrence, D.; Lindsay, K.; Lipscomb, W. H.; Long, M. C.; Mahowald, N.; Marsh, D. R.; Neale, R. B.; Rasch, P.; Vavrus, S.; Vertenstein, M.; Bader, D.; Collins, W. D.; Hack, J. J.; Kiehl, J.; Marshall, S. The Community Earth System Model: A Framework for Collaborative Research. *Bull. Am. Meteorol. Soc.* **2013**, *94* (9), 1339–1360. https://doi.org/10.1175/bams-d-12-00121.1.
(33) Peng, Y.; Yu, P.; Portmann, R. W.; Rosenlof, K. H.; Zhang, J.; Liu, C.; Li, J.; Tian, W. Perturbation of Tropical Stratospheric Ozone Through Homogeneous and Heterogeneous Chemistry Due To Pinatubo. *Geophys. Res. Lett.* **2023**, *50* (16), 1–10. https://doi.org/10.1029/2023gl103773.
(34) Murphy, D. M.; Koop, T. Review of the Vapour Pressures of Ice and Supercooled Water for Atmospheric Applications. *Q. J. R. Meteorol. Soc.* **2005**, *131* (608), 1539–1565.
(35) Yu, P.; Toon, O. B.; Bardeen, C. G.; Zhu, Y.; Rosenlof, K. H.; Portmann, R. W.; Thornberry, T. D.; Gao, R.; Davis, S. M.; Wolf, E. T.; Gouw, J. De; Peterson, D. A. Black Carbon Lofts Wildfire Smokehigh into the Stratosphere to Form Apersistent Plume. *Science* **2019**, *365* (6453), 587–590.
(36) Lambe, A. T.; Onasch, T. B.; Massoli, P.; Croasdale, D. R.; Wright, J. P.; Ahern, A. T.; Williams, L. R.; Worsnop, D. R.; Brune, W. H.; Davidovits, P. Laboratory Studies of the Chemical Composition and Cloud Condensation Nuclei (CCN) Activity of Secondary Organic Aerosol (SOA) and Oxidized Primary Organic Aerosol (OPOA). *Atmos. Chem. Phys.* **2011**, *11* (17), 8913–8928. https://doi.org/10.5194/acp-11-8913-2011.
(37) Li, Y.; A. Day, D.; Stark, H.; L. Jimenez, J.; Shiraiwa, M. Predictions of the Glass Transition Temperature and Viscosity of Organic Aerosols from Volatility Distributions. *Atmos. Chem. Phys.* **2020**, *20* (13), 8103–8122. https://doi.org/10.5194/acp-20-8103-2020.
(38) Hennigan, C. J.; Miracolo, M. A.; Engelhart, G. J.; May, A. A.; Presto, A. A.; Lee, T.; Sullivan, A. P.; McMeeking, G. R.; Coe, H.; Wold, C. E.; Hao, W. M.; Gilman, J. B.;

https://doi.org/10.26434/chemrxiv-2024-27934-v4 **ORCID:** https://orcid.org/0000-0002-5621-2323 Content not peer-reviewed by ChemRxiv. **License:** CC BY 4.0

Kuster, W. C.; De Gouw, J.; Schichtel, B. A.; Collett, J. L.; Kreidenweis, S. M.; Robinson, A. L. Chemical and Physical Transformations of Organic Aerosol from the Photo-Oxidation of Open Biomass Burning Emissions in an Environmental Chamber. *Atmos. Chem. Phys.* **2011**, *11* (15), 7669–7686. https://doi.org/10.5194/acp-11-7669-2011.

(39) Chen, J. M.; Li, C. L.; Ristovski, Z.; Milic, A.; Gu, Y. T.; Islam, M. S.; Wang, S. X.; Hao, J. M.; Zhang, H. F.; He, C. R.; Guo, H.; Fu, H. B.; Miljevic, B.; Morawska, L.; Thai, P.; Fat, L.; Pereira, G.; Ding, A. J.; Huang, X.; Dumka, U. C. A Review of Biomass Burning: Emissions and Impacts on Air Quality, Health and Climate in China. *Sci. Total Environ.* **2016**, *579* (2017), 1000–1034. https://doi.org/10.1016/j.scitotenv.2016.11.025.

(40) Dette, H. P.; Qi, M.; Schröder, D. C.; Godt, A.; Koop, T. Glass-Forming Properties of 3-Methylbutane-1,2,3-Tricarboxylic Acid and Its Mixtures with Water and Pinonic Acid. *J. Phys. Chem. A* **2014**, *118* (34), 7024–7033. https://doi.org/10.1021/jp505910w.

(41) Dette, H. P.; Koop, T. Glass Formation Processes in Mixed Inorganic/Organic Aerosol Particles. *J Phys Chem A* **2015**, *119* (19), 4552–4561. https://doi.org/10.1021/jp5106967.

(42) Kohl, I.; Bachmann, L.; Hallbrucker, A.; Mayer, E.; Loerting, T. Liquid-like Relaxation in Hyperquenched Water at ≤140 K. *Phys. Chem. Chem. Phys.* **2005**, *7* (17), 3210–3220.

(43) C. A. Angell. Relaxation in Liquids, Polymers and Plastic Crystals - Strong/Fragile Patterns and Problems. *J. Non. Cryst. Solids* **1991**, *131*, 13–31.

(44) Kiland, K. J.; Mahrt, F.; Peng, L.; Nikkho, S.; Zaks, J.; Crescenzo, G. V.; Bertram, A. K. Viscosity, Glass Formation, and Mixing Times within Secondary Organic Aerosol from Biomass Burning Phenolics. *ACS Earth Sp. Chem.* **2023**, *7* (7), 1388–1400.

(45) Al-Mashala, H. H.; Betz, K. L.; Calvert, C. T.; Barton, J. A.; Bruce, E. E.; Schnitzler, E. G. Ultraviolet Irradiation Can Increase the Light Absorption and Viscosity of Primary Brown Carbon from Biomass Burning. *ACS Earth Sp. Chem.* **2023**, *7* (10), 1882–1889. https://doi.org/10.1021/acsearthspacechem.3c00155.

(46) Xie, Q.; Gerrebos, N. G. A.; Calderon-Arrieta, D.; Morton, I. S.; Halpern, E.; Li, C.; Zeng, M. F.; Bertram, A. K.; Rudich, Y.; Laskin, A. Molecular Insights into Gas-Particle Partitioning and Viscosity of Atmospheric Brown Carbon. *Environ. Sci. Technol.* **2024**, *58* (41), 18484–18294. https://doi.org/10.1021/acs.est.4c05650.

(47) Gervasi, N. R.; Topping, D. O.; Zuend, A. A Predictive Group-Contribution Model for the Viscosity of Aqueous Organic Aerosol. *Atmos. Chem. Phys.* **2020**, *20* (5), 2987–3008. https://doi.org/10.5194/acp-20-2987-2020.

(48) Lilek, J.; Zuend, A. A Predictive Viscosity Model for Aqueous Electrolytes and Mixed Organic-Inorganic Aerosol Phases. *Atmos. Chem. Phys.* **2022**, *22* (5), 3203–3233. https://doi.org/10.5194/acp-22-3203-2022.

(49) Song, Y. C.; Lilek, J.; Lee, J. B.; Chan, M. N.; Wu, Z.; Zuend, A.; Song, M. Viscosity and Phase State of Aerosol Particles Consisting of Sucrose Mixed with Inorganic Salts. *Atmos. Chem. Phys.* **2021**, *21* (13), 10215–10228. https://doi.org/10.5194/acp-21-10215-2021.

(50) Thompson, C. R.; Wofsy, S. C.; Prather, M. J.; Newman, P. A.; Hanisco, T. F.; Ryerson, T. B.; Fahey, D. W.; Apel, E. C.; Brock, C. A.; Brune, W. H.; Froyd, K.; Katich, J. M.; Nicely, J. M.; Peischl, J.; Ray, E.; Veres, P. R.; Wang, S.; Allen, H. M.; Asher, E.; Bian, H.; Blake, D.; Bourgeois, I.; Budney, J.; Paul Bui, T.; Butler, A.; Campuzano-Jost, P.; Chang, C.; Chin, M.; Commane, R.; Correa, G.; Crounse, J. D.; Daube, B.; Dibb, J. E.; DiGangi, J. P.; Diskin, G. S.; Dollner, M.; Elkins, J. W.; Fiore, A. M.; Flynn, C. M.; Guo, H.; Hall, S. R.; Hannun, R. A.; Hills, A.; Hintsa, E. J.; Hodzic, A.; Hornbrook, R. S.; Greg Huey, L.; Jimenez, J. L.; Keeling, R. F.; Kim, M. J.; Kupc, A.; Lacey, F.; Lait, L. R.;

https://doi.org/10.26434/chemrxiv-2024-27934-v4 **ORCID:** https://orcid.org/0000-0002-5621-2323 Content not peer-reviewed by ChemRxiv. **License:** CC BY 4.0

Lamarque, J. F.; Liu, J.; McKain, K.; Meinardi, S.; Miller, D. O.; Montzka, S. A.; Moore, F. L.; Morgan, E. J.; Murphy, D. M.; Murray, L. T.; Nault, B. A.; Andrew Neuman, J.; Nguyen, L.; Gonzalez, Y.; Rollins, A.; Rosenlof, K.; Sargent, M.; Schill, G.; Schwarz, J. P.; St. Clair, J. M.; Steenrod, S. D.; Stephens, B. B.; Strahan, S. E.; Strode, S. A.; Sweeney, C.; Thames, A. B.; Ullmann, K.; Wagner, N.; Weber, R.; Weinzierl, B.; Wennberg, P. O.; Williamson, C. J.; Wolfe, G. M.; Zeng, L. The NASA Atmospheric Tomography (ATom) Mission: Imaging the Chemistry of the Global Atmosphere. *Bull. Am. Meteorol. Soc.* **2022**, *103* (3), 761–790. https://doi.org/10.1175/BAMS-D-20-0315.1.

(51) Katich, J. M.; Apel, E. C.; Bourgeois, I.; Brock, C. A.; Bui, T. P.; Campuzano-Jost, P.; Commane, R.; Daube, B.; Dollner, M.; Fromm, M.; Froyd, K. D.; Hills, A. J.; Hornbrook, R. S.; Jimenez, J. L.; Kupc, A.; Lamb, K. D.; McKain, K.; Moore, F.; Murphy, D. M.; Nault, B. A.; Peischl, J.; Perring, A. E.; Peterson, D. A.; Ray, E. A.; Rosenlof, K. H.; Ryerson, T.; Schill, G. P.; Schroder, J. C.; Weinzierl, B.; Thompson, C.; Williamson, C. J.; Wofsy, S. C.; Yu, P.; Schwarz, J. P. Pyrocumulonimbus Affect Average Stratospheric Aerosol Composition. *Science* **2023**, *379* (6634), 815–820. https://doi.org/10.1126/science.add3101.

(52) Froyd, K. D.; Murphy, D. M.; Brock, C. A.; Campuzano-Jost, P.; Dibb, J. E.; Jimenez, J.-L.; Kupc, A.; Middlebrook, A. M.; Schill, G. P.; Thornhill, K. L.; Williamson, C. J.; Wilson, J. C.; Ziemba, L. D. A New Method to Quantify Mineral Dust and Other Aerosol Species from Aircraft Platforms Using Single-Particle Mass Spectrometry. *Atmos. Meas. Tech.* **2019**, *12* (11), 6209–6239. https://doi.org/10.5194/amt-12-6209-2019.

(53) Reid, J. P.; Bertram, A. K.; Topping, D. O.; Laskin, A.; Martin, S. T.; Petters, M. D.; Pope, F. D.; Rovelli, G. The Viscosity of Atmospherically Relevant Organic Particles. *Nat. Commun.* **2018**, *9* (956), 1–14.

(54) Ruzmaikin, A.; Aumann, H. H.; Manning, E. M. Relative Humidity in the Troposphere with AIRS. *J. Atmos. Sci.* **2014**, *71* (7), 2516–2533. https://doi.org/10.1175/JAS-D-13-0363.1.

(55) Haarig, M.; Ansmann, A.; Baars, H.; Jimenez, C.; Veselovskii, I.; Engelmann, R.; Althausen, D. Depolarization and Lidar Ratios at 355, 532, and 1064nm and Microphysical Properties of Aged Tropospheric and Stratospheric Canadian Wildfire Smoke. *Atmos. Chem. Phys.* **2018**, *18* (16), 11847–11861. https://doi.org/10.5194/acp-18-11847-2018.

(56) Hu, Q.; Goloub, P.; Veselovskii, I.; Bravo-Aranda, J.-A.; Popovici, I. E.; Podvin, T.; Haeffelin, M.; Lopatin, A.; Dubovik, O.; Pietras, C.; Huang, X.; Torres, B.; Chen, C. Long-Range-Transported Canadian Smoke Plumes in the Lower Stratosphere over Northern France. *Atmos. Chem. Phys. 19* (2), 1173–1193. https://doi.org/10.5194/acp-19-1173-2019.

(57) Ohneiser, K.; Ansmann, A.; Baars, H.; Seifert, P.; Barja, B.; Jimenez, C.; Radenz, M.; Teisseire, A.; Floutsi, A.; Haarig, M.; Foth, A.; Chudnovsky, A.; Engelmann, R.; Zamorano, F.; Buhl, J.; Wandinger, U. Smoke of Extreme Australian Bushfires Observed in the Stratosphere over Punta Arenas, Chile, in January 2020: Optical Thickness, Lidar Ratios, and Depolarization Ratios at 355 and 532nm. *Atmos. Chem. Phys.* **2020**, *20* (13), 8003–8015. https://doi.org/10.5194/acp-20-8003-2020.

(58) June, N. A.; Hodshire, A. L.; Wiggins, E. B.; Winstead, E. L.; Robinson, C. E.; Thornhill, K. L.; Sanchez, K. J.; Moore, R. H.; Pagonis, D.; Guo, H.; Campuzano-Jost, P.; Jimenez, J. L.; Coggon, M. M.; Dean-Day, J. M.; Bui, T. P.; Peischl, J.; Yokelson, R. J.; Alvarado,

https://doi.org/10.26434/chemrxiv-2024-27934-v4 **ORCID:** https://orcid.org/0000-0002-5621-2323 Content not peer-reviewed by ChemRxiv. **License:** CC BY 4.0

M. J.; Kreidenweis, S. M.; Jathar, S. H.; Pierce, J. R. Aerosol Size Distribution Changes in FIREX-AQ Biomass Burning Plumes: The Impact of Plume Concentration on Coagulation and OA Condensation/Evaporation. *Atmos. Chem. Phys.* **2022**, *22* (19), 12803–12825. https://doi.org/10.5194/acp-22-12803-2022.

(59) Järvinen, E.; Ignatius, K.; Nichman, L.; Kristensen, T. B.; Fuchs, C.; Hoyle, C. R.; Höppel, N.; Corbin, J. C.; Craven, J.; Duplissy, J.; Ehrhart, S.; El Haddad, I.; Frege, C.; Gordon, H.; Jokinen, T.; Kallinger, P.; Kirkby, J.; Kiselev, A.; Naumann, K.-H.; Petäjä, T.; Pinterich, T.; Prevot, A. S. H.; Saathoff, H.; Schiebel, T.; Sengupta, K.; Simon, M.; Slowik, J. G.; Tröstl, J.; Virtanen, A.; Vochezer, P.; Vogt, S.; Wagner, A. C.; Wagner, R.; Williamson, C.; Winkler, P. M.; Yan, C.; Baltensperger, U.; Donahue, N. M.; Flagan, R. C.; Gallagher, M.; Hansel, A.; Kulmala, M.; Stratmann, F.; Worsnop, D. R.; Möhler, O.; Leisner, T.; Schnaiter, M. Observation of Viscosity Transition in Alpha-Pinene Secondary Organic Aerosol. *Atmos. Chem. Phys.* **2016**, *16* (7), 4423–4438. https://doi.org/10.5194/acp-16-4423-2016.

(60) Girotto, G.; China, S.; Bhandari, J.; Gorkowski, K.; Scarnato, B. V.; Capek, T.; Marinoni, A.; Veghte, D. P.; Kulkarni, G.; Aiken, A. C.; Dubey, M.; Mazzoleni, C. Fractal-like Tar Ball Aggregates from Wildfire Smoke. *Environ. Sci. Technol. Lett.* **2018**, *5* (6), 360–365. https://doi.org/10.1021/acs.estlett.8b00229.

(61) Liu, L.; Mishchenko, M. I. Modeling Study of Scattering and Absorption Properties of Tar-Ball Aggregates. *Appl Opt* **2019**, *58* (31), 8648–8657. https://doi.org/10.1364/AO.58.008648.

(62) Leung, K. K.; Schnitzler, E. G.; Jäger, W.; Olfert, J. S. Relative Humidity Dependence of Soot Aggregate Restructuring Induced by Secondary Organic Aerosol: Effects of Water on Coating Viscosity and Surface Tension. *Environ. Sci. Technol. Lett.* **2017**, *4* (9), 386–390. https://doi.org/10.1021/acs.estlett.7b00298.

(63) Ohneiser, K.; Ansmann, A.; Kaifler, B.; Chudnovsky, A.; Barja, B.; Knopf, D. A.; Kaifler, N.; Baars, H.; Seifert, P.; Villanueva, D.; Jimenez, C.; Radenz, M.; Engelmann, R.; Veselovskii, I.; Zamorano, F. Australian Wildfire Smoke in the Stratosphere: The Decay Phase in 2020/2021 and Impact on Ozone Depletion. *Atmos. Chem. Phys.* **2022**, *22* (11), 7417–7442. https://doi.org/10.5194/acp-22-7417-2022.

(64) Ijaz, A.; Kew, W.; Cheng, Z.; Mathai, S.; Lata, N. N.; Kovarik, L.; Schum, S.; China, S.; Mazzoleni, L. R. Molecular and Physical Composition of Tar Balls in Wildfire Smoke: An Investigation with Complementary Ionisation Methods and 15-Tesla FT-ICR Mass Spectrometry. *Environ. Sci. Atmos.* **2023**, *3* (10), 1552–1562. https://doi.org/10.1039/d3ea00085k.

(65) Sedlacek, A. J.; Buseck, P. R.; Adachi, K.; Onasch, T. B.; Springston, S. R.; Kleinman, L. Formation and Evolution of Tar Balls from Northwestern US Wildfires. *Atmos. Chem. Phys.* **2018**, *18* (15), 11289–11301. https://doi.org/10.5194/acp-18-11289-2018.

(66) Song, M.; Marcolli, C.; Krieger, U. K.; Zuend, A.; Peter, T. Liquid-Liquid Phase Separation in Aerosol Particles: Dependence on O:C, Organic Functionalities, and Compositional Complexity. *Geophys. Res. Lett.* **2012**, *39* (19), 1–5. https://doi.org/10.1029/2012GL052807.

(67) You, Y.; Smith, M. L.; Song, M.; Martin, S. T.; Bertram, A. K. Liquid-Liquid Phase Separation in Atmospherically Relevant Particles Consisting of Organic Species and Inorganic Salts. *Int. Rev. Phys. Chem.* **2014**, *33* (1), 43–77. https://doi.org/10.1080/0144235X.2014.890786.

https://doi.org/10.26434/chemrxiv-2024-27934-v4 **ORCID:** https://orcid.org/0000-0002-5621-2323 Content not peer-reviewed by ChemRxiv. **License:** CC BY 4.0

(68) Freedman, M. A. Phase Separation in Organic Aerosol. *Chem. Soc. Rev.* **2017**, *46* (24), 7694–7705. https://doi.org/10.1039/c6cs00783j.
(69) Knopf, D. A.; Alpert, P. A.; Wang, B. The Role of Organic Aerosol in Atmospheric Ice Nucleation: A Review. *ACS Earth Sp. Chem.* **2018**, *2* (3), 168–202. https://doi.org/10.1021/acsearthspacechem.7b00120.
(70) Wolf, M. J.; Zhang, Y.; Zawadowicz, M. A.; Goodell, M.; Froyd, K.; Freney, E.; Sellegri, K.; Rösch, M.; Cui, T.; Winter, M.; Lacher, L.; Axisa, D.; DeMott, P. J.; Levin, E. J. T.; Gute, E.; Abbatt, J.; Koss, A.; Kroll, J. H.; Surratt, J. D.; Cziczo, D. J. A Biogenic Secondary Organic Aerosol Source of Cirrus Ice Nucleating Particles. *Nat. Commun.* **2020**, *11* (1), 4834. https://doi.org/10.1038/s41467-020-18424-6.
(71) Murray, B. J.; Wilson, T. W.; Dobbie, S.; Cui, Z. Q.; Al-Jumur, S.; Mohler, O.; Schnaiter, M.; Wagner, R.; Benz, S.; Niemand, M.; Saathoff, H.; Ebert, V.; Wagner, S.; Karcher, B. Heterogeneous Nucleation of Ice Particles on Glassy Aerosols under Cirrus Conditions. *Nat. Geosci.* **2010**, *3* (4), 233–237. https://doi.org/10.1038/ngeo817.
(72) Schill, G. P.; Tolbert, M. A. Heterogeneous Ice Nucleation on Phase-Separated Organic-Sulfate Particles: Effect of Liquid vs. Glassy Coatings. *Atmos. Chem. Phys.* **2013**, *13* (9), 4681–4695. https://doi.org/10.5194/acp-13-4681-2013.
(73) Kasparoglu, S.; Perkins, R.; Ziemann, P. J.; DeMott, P. J.; Kreidenweis, S. M.; Finewax, Z.; Deming, B. L.; DeVault, M. P.; Petters, M. D. Experimental Determination of the Relationship Between Organic Aerosol Viscosity and Ice Nucleation at Upper Free Tropospheric Conditions. *J. Geophys. Res. Atmos.* **2022**, *127* (16), 1–20. https://doi.org/10.1029/2021JD036296.
(74) Carslaw, K. S.; Luo, B. P.; Clegg, S. L.; Peter, T.; Brimblecombe, P.; Crutzen, P. J. Stratospheric Aerosol Growth and HNO_3 Gas Phase Depletion from Coupled HNO_3 and Water Uptake by Liquid Particles. *Geophys. Res. Lett.* **1994**, *21* (23), 2479–2482. https://doi.org/10.1029/94GL02799.

For Table of Contents Only

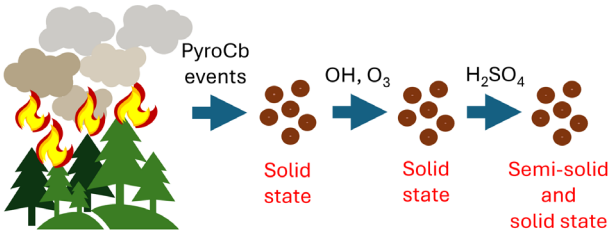

Phase state of wildfire smoke in the stratosphere at 250 — 205 K and 15 — 32 km.

https://doi.org/10.26434/chemrxiv-2024-27934-v4 **ORCID:** https://orcid.org/0000-0002-5621-2323 Content not peer-reviewed by ChemRxiv. **License:** CC BY 4.0